Platinum Complexes

Deutsche Ausgabe: DOI: 10.1002/ange.201502390
Internationale Ausgabe: DOI: 10.1002/anie.201502390

The Role of Substituent Effects in Tuning Metallophilic Interactions and Emission Energy of Bis-4-(2-pyridyl)-1,2,3-triazolatoplatinum(II) Complexes**

*M. R. Ranga Prabhath, Julia Romanova, Richard J. Curry, S. Ravi P. Silva, and Peter D. Jarowski**

Abstract: *The photoluminescence spectra of a series of 5-substituted pyridyl-1,2,3-triazolato Pt^{II} homoleptic complexes show weak emission tunability (ranging from $\lambda = 397$–408 nm) in dilute (10^{-6} M) ethanolic solutions at the monomer level and strong tunability in concentrated solutions (10^{-4} M) and thin films (ranging from $\lambda = 487$–625 nm) from dimeric excited states (excimers). The results of density functional calculations (PBE0) attribute this "turn-on" sensitivity and intensity in the excimer to strong Pt–Pt metallophilic interactions and a change in the excited-state character from singlet metal-to-ligand charge transfer (^{1}MLCT) to singlet metal-metal-to-ligand charge transfer (^{1}MMLCT) emissions in agreement with lifetime measurements.*

Owing to superior energy efficiency, light emitting diode (LED) technology has become considerably commercialized over the last decade.[1] For organic LEDs (OLEDs), innovations have been spurred along by the discovery of new molecules with good stability and high emission intensity, followed through by intense engineering efforts. Heavy-metal-containing complexes are potent molecular emitters as a result of their high quantum efficiencies (QEs, ϕ) related to facile intersystem crossing (ISC) between excited-state manifolds (efficient spin orbit coupling (SOC)) and resultant efficient emission from the triplet state (phosphorescence).[2] Rational tuning of the emission wavelengths based on structural modifications of the ligands,[3] with concomitant control of the QE, has been demonstrated in a number of octahedral complexes of d^6 metals[4] including predominantly iridium,[4a,b] rhodium,[4c] and ruthenium[4d] and with a large range of structurally diverse ligands. The square-planar d^8 complexes have also received considerable interest since the seminal work of Gray, Vlcek, Miskowski, and co-workers.[5] Square-planar platinum complexes present excellent emissive properties and allow for a more minimal planar structural motif with less diasteromeric diversity. However, anticipated deleterious excitonic self-quenching of planar complexes brought on by enhanced intermolecular electronic coupling through π–π stacking interactions implies considerable design difficulties for this class of phosphors. Nonetheless, for Pt^{II} complexes this negative aspect is largely offset by the propensity of these systems to engage in metallophilic Pt–Pt interactions. These interactions give rise to new and interesting photophysics involving transitions between metallophilic bonds and ligands, denoted metal-metal-to-ligand charge transfer (MMLCT), providing supramolecular design potential for further property tunability.[6] Indeed, a number of studies have shown strong emission intensity despite clear metallophilic stacking.[7] A better understanding and control of such interactions may lead to materials with increased quantum yields and potential anisotropic ordering arranged through discrete noncovalent interactions. Further studies of the excimer states of such systems through systematic alteration of the ligands would reveal important design criteria towards these goals.

In this study the photophysical properties of novel pyridyltriazolate complexes of platinum(II) are explored. Compared to other pyridyl azoles,[7a,8] pyridyl-1,2,3-triazoles are less studied. Moreover, most of the examples related to pyridyl-1,2,3-triazoles involve substitution at the N atom of the triazolyl ring, which should affect the energy of the highest occupied molecular orbital (HOMO). However, triazole is electronically insulating and thus substituent effects have not been very pronounced.[9] A more effective tuning route might target the lowest unoccupied molecular orbital (LUMO) that is located on the pyridyl ring and is anticipated to be more closely associated with the excited state.[8b] Thus, in the present work, pyridyl-1*H*-1,2,3-triazole ligands were prepared using efficient reactions to build a structurally homologous series of donor and acceptor 5-pyridyl-substituted anionic ligands. These ligands were prepared by deprotonation of the 1*H*-triazolyl moiety to give strong-field ligation (suppressed d–d transitions)[10] in the neutral final complexes (Scheme 1). Keeping synthetic efficiency in mind, the target ligands were approached through the serial application of the Sonogashira carbon–carbon coupling[11a] and the Sharpless copper-catalyzed Huisgen's 1,3-dipolar cycloaddition procedures (see the Supporting Information, Sections S1 and S2 for experimental procedures).[11b] Starting from the 2-bromopyridyl derivatives **1a** ($R = NMe_2$), **1b** ($R = H$), and **1c** ($R = CHO$), Sonogashira coupling with trimethyl-

[*] M. R. R. Prabhath, Dr. J. Romanova, Prof. R. J. Curry, Prof. S. R. P. Silva, Dr. P. D. Jarowski
University of Surrey, Advanced Technology Institute
Guildford, GU2 7XH (UK)
E-mail: p.d.jarowski@surrey.ac.uk

[**] We would like to thank the EPSRC (EP/K009664/1) (UK), a Royal Society Research Grant (RG11041), and the Leverhulme Trust (RPG-2014-006) for funding as well as the National Service for Computational Chemistry Software (NSCCS) at Imperial College London and the National MS Service. M.R.R.P. would like to thank the Southeast Physics Network (SEPnet) for student funding.

Supporting information for this article is available on the WWW under http://dx.doi.org/10.1002/anie.201502390.

 © 2015 Wiley-VCH Verlag GmbH & Co. KGaA, Weinheim

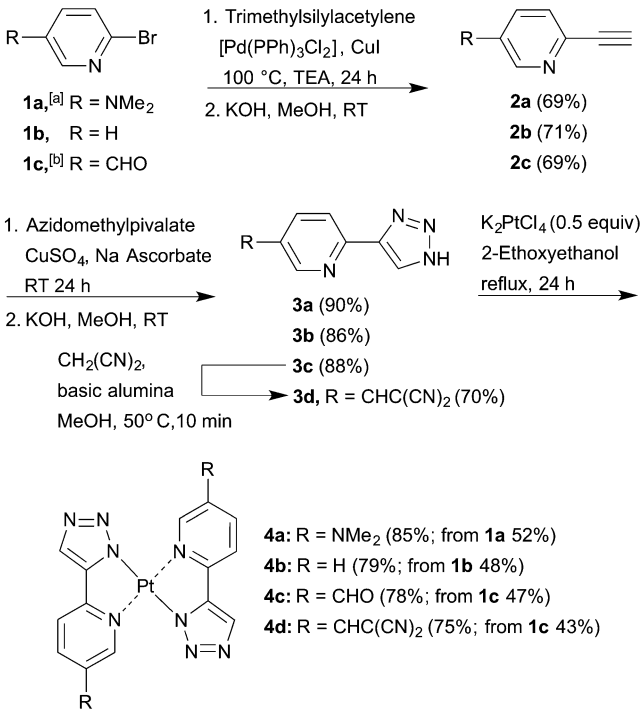

Scheme 1. Synthesis of the pyridyl-1*H*-1,2,3-triazole ligands **3a–3d** and resultant homoleptic Pt^{II} complexes **4a–d**. [a] Prepared from *N*,*N*-dimethylpyridine-3-amine, and [b] prepared from 2,5-dibromopyridine (Supporting Information, Section S2). TEA = triethylamine.

silylacetylene produced the terminal alkynylated pyridines (**2a–c**) in approximately 70% yield after nearly quantitative basic desilylation with KOH. Following this, copper-catalyzed reaction of these terminal alkynes with azidomethylpivalate gave the N-protected 1,4-disubstituted-1,2,3-triazoles in circa 90% yield with subsequent quantitative deprotection yielding the intended 1*H*-1,2,3-triazole ligands (**3a–c**). Ligand **3d** (R = $CHC(CN)_2$) was synthesized from **3c** by Knoevenagel condensation with malononitrile in the presence of catalytic basic alumina.[11c] Platinum complexes **4a–d** were then prepared by refluxing two equivalents of these ligands in basic 2-ethoxyethanol in the presence of K_2PtCl_4 resulting in a sparsely soluble powder, which was subsequently washed in ethanol and acetone to give the homoleptic complexes (see Section S3 in the Supporting Information).

The complexes were characterized by electrospray ionization mass spectrometry (ESI-MS) and ^{1}H NMR spectroscopy. In the ^{1}H NMR spectra, significant shifts of signals attributable to protons on complexes **4a–d** compared to those of ligands **3a–d** indicate clear deshielding effects of the ligand protons (Figures S4) induced by the electron-accepting platinum ion. This effect has been found in studies on related systems although the sparse solubility[12] and broadening effect from platinum render the recorded spectra poorly resolved.[13] The complexation process is confirmed further, however, by analysis of IR spectral shifts associated with C–H vibronic bands on the pyridyl rings (Figures S5) and by analysis of the UV/Vis electronic absorption spectra (Figures S6). Solubility problems were compounded for ^{13}C NMR spectroscopy, which is not presented along with issues with the elemental analysis, which gave uninterpretable results, presumably as a result of platinum carbide combustion products. Overall yields, starting from **1**, were in the range of 27–52%, making these complexes scalable for industrial use. Theoretical calculations were performed with density functional theory (DFT) and its time-dependent (TD) formalism by using the PBE0 functional, 6-31G(d) basis set for the ligands, and SDD basis set for the Pt atoms. The polarizable continuum model (PCM) in its integral equation formalism variant was employed to take into account the solvent effects. Details of the computational procedure and the corresponding references can be found in the Supporting Information (Section S7).

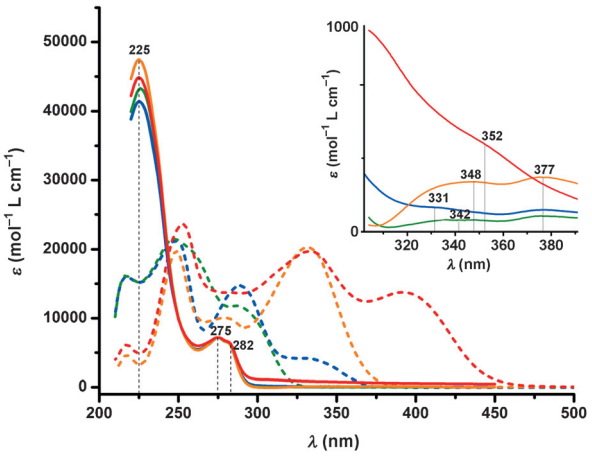

Figure 1. UV/Vis absorption spectra (10^{-5} M in ethanol) of free ligands (-----; in basic solution) and platinum complexes (——). **3a/4a** (blue), **3b/4b** (green), **3c/4c** (orange), and **3d/4d** (red). Inset: Expanded low-energy absorption spectra of complexes **4** from λ = 300–390 nm.

The UV/Vis absorption spectra of the free ligands (**3a–d**) are given in Figure 1 in basic ethanolic solutions (10^{-5} M) so that the triazolate is formed for direct comparison of the free ligand to the complexed ligand. Based on the structure of the free ligands, the molecules are expected to exhibit intramolecular charge-transfer properties with the cyclic amino group of the triazolate donating to the electron-accepting pyridine ring and its substituent with an associated red shift following the Hammett parameters of the substituents (σ_p).[14] Indeed, the lowest-energy absorption band undergoes a red shift with increasing electron-acceptor ability (total range $\Delta\lambda$ = 104 nm) from λ = 288 nm (**3b**, σ_p = 0), 333 nm (**3c**, σ_p = 0.42), and 392 nm (**3d**, σ_p = 0.84), whereas the introduction of a donating group (**3a**, σ_p = −0.83) gives rise to a lowest-energy absorption band at λ = 332 nm. The experimentally observed trend is also confirmed by DFT PBE0 calculations, which predict the lowest-energy absorption bands at λ = 281 nm (**3b**), 338 nm (**3c**), 421 nm (**3d**), and 313 nm (**3a**) (Table S8). Moreover, the analysis of the molecular orbitals (MO) clearly indicates the charge-transfer character of these transitions (Section S9). In addition to the most red-shifted absorption bands, similar transitions are experimentally observed for all free ligands at circa λ = 280, 250, and 220 nm with relatively less sensitivity to substitution.

 © 2015 Wiley-VCH Verlag GmbH & Co. KGaA, Weinheim

Homoleptic complexes of these ligands with platinum, **4a–d**, in ethanolic solutions (10^{-5} M) exhibit low-energy absorption bands ranging from $\lambda = 300$ nm to 400 nm with values of 331 nm and 377 nm (**4a**), 342 nm and 377 nm (**4b**), 348 nm and 377 nm (**4c**), and 352 nm (**4d**; an inflection point is also detected at circa 370 nm for this complex). These bands indicate a lowered tunability with changing substituent with a range of only a few nanometers for shifts of lowest-energy absorption bands. The lowered tunability is also confirmed by PBE0 results (Table S10), which reveal absorption bands located at $\lambda = 311$ nm and 376 nm (**4a**), 301 nm and 338 nm (**4b**), 326 nm and 370 nm (**4c**), as well as at 365 nm and 416 nm (**4d**). MO analysis identifies these bands as having metal-to-ligand charge-transfer character (^{1}MLCT) involving the d_{xz} and d_{yz} orbitals (Section S11). The complexes also present intense high-energy absorption bands that are nearly overlaid and are found at circa $\lambda = 275$ nm followed by a shoulder at approximately 282 nm. Completing the UV/Vis absorption spectra are intense bands at circa $\lambda = 225$ nm. These high-energy bands appear to be associated with the free-ligand bands at circa $\lambda = 280$ nm and 250 nm, both with hypsochromic shifts. Upon increasing the concentration of the ethanolic solutions, UV/Vis absorption spectra for the free ligands and complexes obey the Beer–Lambert Law.

The photoluminescence (PL) spectra of the free ligands (Figure 2; dashed lines) were measured in ethanol (10^{-6} M; $\lambda_{exc} = 350$ nm). Ligands **3a** and **3b** exhibited similar emission spectra with emission maxima centered at $\lambda = 400$ nm and 402 nm, respectively. In contrast, a considerable bathochromic shift was detected for the emission of ligands **3c** (431 nm) and **3d** (469 nm). These PL bands are overlapped with the lowest-energy absorption bands. The emission lifetime for **3b** was measured in thin film ($\lambda = 390$ nm) as < 16 ns and is associated with fluorescence. PL spectra of dilute solutions (10^{-6} M) of the complexes recorded at the same excitation wavelength, however, display very similar emission maxima for **4a** ($\lambda = 397$ nm), **4b** (400 nm), **4c** (405 nm), and **4d** (408 nm; Figure 2). Additionally, for **4a** and **4b** the emission profile and maxima are strikingly similar to those of their corresponding ligands **3a** and **3b** whereas for **4c** and **4d** the emission maxima of the complexes are blue shifted compared to **3c** and **3d**. Emission spectra centered around $\lambda = 400$ nm allow for good spectral overlap with the lowest-energy absorption bands of the complexes as well, which are in the 300 to 400 nm range, pointing to fluorescence despite the proximity and strong interaction of the ligand with the heavy platinum cation. Assignment of this emission as fluorescence is also in accordance with the measured emission lifetime for **4b** in dilute solution (at $\lambda = 390$ nm) which was found to be < 15 ns. Time-dependent DFT (TDDFT) excited-state optimizations have been performed for the lowest singlet (S_1) and triplet (T_1, T_2) states of the complexes (Sections S13 and S14). The results indicate good qualitative agreement between the experimental PL maxima (Figure 2) and the calculated $S_1 \rightarrow S_0$ emission energies: $\lambda = 416$ nm (**4a**), 375 nm (**4b**), 413 nm (**4c**), and 461 nm (**4d**). In contrast, the predicted phosphorescence energies are considerable lower in energy and do not follow the experimentally measured qualitative trend in range or ordering ($\lambda = 686$ nm (**4a**), 473 nm (**4b**), 517 nm (**4c**), and 956 nm (**4d**)). Therefore, these values should not be related to the observed emissive processes. Thus, the computational and experimental results together identify the emission at the molecular level as fluorescence derived from a ^{1}MLCT state. Photoluminescence excitation (PLE) spectra confirm the relationship between the measured absorption and emission spectra (Section S6).

Key to our findings, however, is that the substituent effects on the emission properties are restored in concentrated solutions (10^{-4} M) of the complexes revealing a pronounced tunability (Figure 3). In concentrated solution, lowest-energy emission can be detected across a large portion of the visible spectrum with PL bands found at $\lambda = 459$ nm (**4a**), 540 nm (**4b**), 575 nm (**4c**), and 599 nm (**4d**). The detected tunability in concentrated solution indicates that the aggregation causes a significant change in the excited-state character and suggests the existence of excited dimer

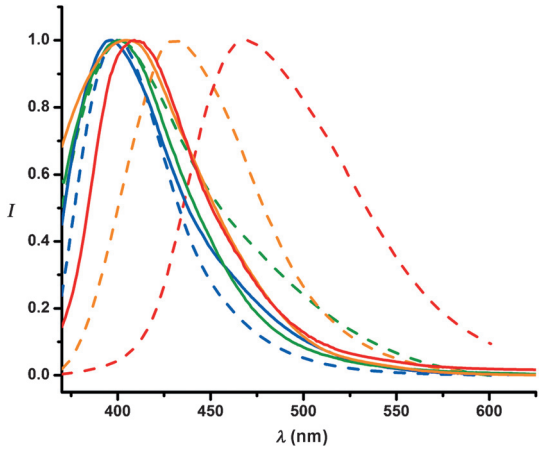

Figure 2. Photoluminescence spectra (10^{-6} M in ethanol; $\lambda_{exc} = 350$ nm) of free ligands (-----) and complexes (——). **3a**/**4a** (blue), **3b**/**4b** (green), **3c**/**4c** (orange), and **3d**/**4d** (red).

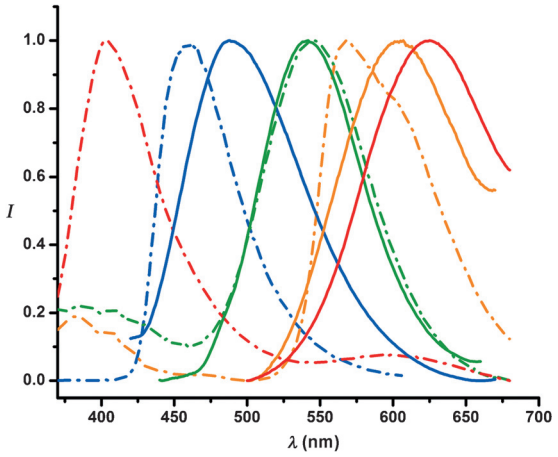

Figure 3. Photoluminescence spectra ($\lambda_{exc} = 350$ nm) of **4a** (blue), **4b** (green), **4c** (orange), and **4d** (red) in solution (-----; 10^{-4} M in ethanol) and as a thin film (——).

© 2015 Wiley-VCH Verlag GmbH & Co. KGaA, Weinheim

(excimer) states. Both monomeric and excimeric emission can be detected for **4b–d** in concentrated solution simultaneously, to different degrees, suggesting that the equilibrium for excimer formation is affected by the substituent with **4a–c** emitting from the excimeric state and **4d** showing a strong residual monomeric emission. PLE spectra for the excimeric emissions show little correspondence to the monomeric absorption and are thus newly generated species (Section S6). For these emission bands, red shifts are increasingly large (from **4a** to **4d**) compared to the lowest energy absorption bands and the spectral overlap correspondingly decreases. In the thin films of the complexes (Figure 3, solid lines), there is an additional, and varying, bathochromic shift of the PL maxima with a comparable range from $\lambda = 487$ nm to 625 nm: **4a** (487 nm), **4b** (541 nm), **4c** (602 nm), and **4d** (625 nm), emitting in the blue, green, orange, and red regions, respectively. A linear relationship between the emission energy (in eV) and the donor–acceptor strength (σ_p) of the substituents was established with an R^2 value of 0.97 ($\rho = -0.4$) for the thin film, suggesting that the tunability is directly related to the nature of the substituents.

To understand the substituent effect at higher concentration, which is absent at lower concentration, theoretical calculations on the **4a–4a**, **4b–4b**, **4c–4c**, and **4d–4d** dimers have been carried out. The results are summarized in Figure 4 (see also Sections S11 and S13) where we have applied the

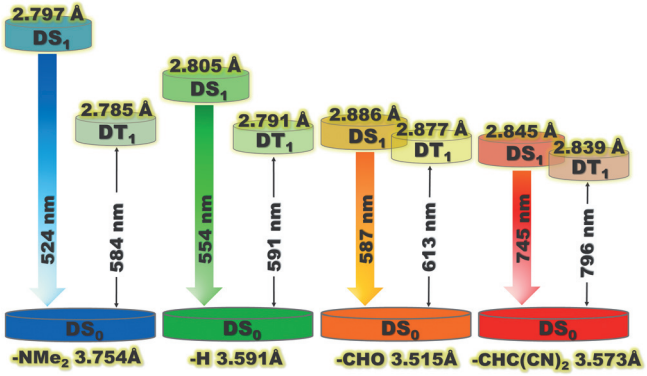

Figure 4. Equilibrium Pt–Pt distances [Å] in the ground (DS_0) and in excimeric states (DS_1, DT_1). $DS_1 \rightarrow DS_0$ and $DT_1 \rightarrow DS_0$ emission wavelengths are given for the dimers of **4a–d** which were obtained with the TDDFT/PBE0 method in ethanol.

chosen level of theory based on recent works.[15] The results indicate that, upon excitation, an enhancement of the metallophilic interaction is found and the Pt–Pt distance (R_{Pt-Pt}) changes from 3.515–3.754 Å in the dimeric ground state DS_0 to 2.791–2.877 Å in the dimeric excimeric singlet (DS_1) and triplet (DT_1) states. Moreover, the significantly shortened Pt–Pt distance in the excited states indicates a covalent interaction (van der Waals radius of Pt ≈ 1.8 Å) and thus confirms the formation of the excimeric states. The molecular-orbital analysis shows that this covalent interaction originates from the sigma-type overlap between the d_{z^2} atomic orbitals of the two Pt centers (Figure 5; Section S15). Indeed, at higher concentration, ^{1}MLCT or ^{3}MLCT emitting states of the

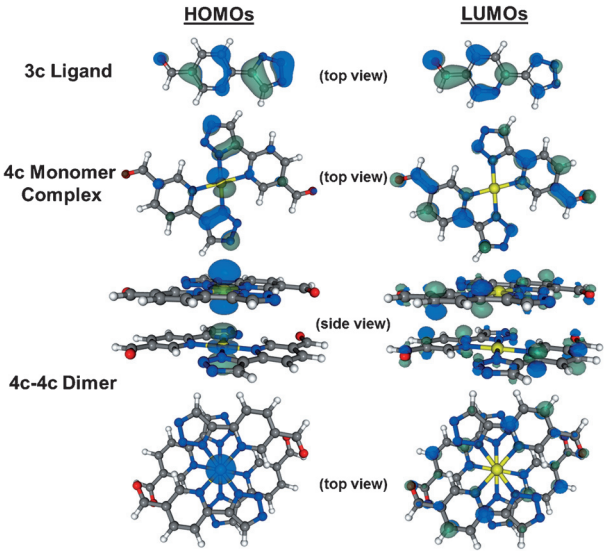

Figure 5. MO representation of the change in the electronic character of the first excited singlet state (HOMO→LUMO transition) going from the isolated ligand **3c** (^{1}ILCT; singlet intraligand charge transfer), to the monomer complex **4c** (^{1}MLCT), and the dimer **4c–4c** (^{1}MMLCT). The molecular orbitals are represented by an isosurface value set to 0.04 a.u.

monomers are replaced by excimeric states with metal-metal-to-ligand charge-transfer character (^{1}MMLCT or ^{3}MMLCT) and the emission is associated with transitions from ligand-centered molecular orbitals to metal-centered molecular orbitals representing the antibonding $(d_{z^2}–d_{z^2})^*$ combination. Moreover, the simulations reveal that because of the excimerization process, the DS_1 state is stabilized with respect to the DT_1 state and that the energy difference between them decreases as a function of the acceptor strength (up to 0.1 eV in **4d–4d**; Figure 4). The quantum-chemical results also reveal better tunability for the $DS_1 \rightarrow DS_0$ emission energies from $\lambda = 524$ nm (**4a–4a**), 554 nm (**4b–4b**), 587 nm (**4c–4c**), to 745 nm (**4d–4d**), and a relatively narrow range of $DT_1 \rightarrow DS_0$ emission energies from 584 nm (**4a–4a**), 591 nm (**4b–4b**), to 613 nm (**4c–4c**). The computed value of 796 nm (**4d–4d**) for $DT_1 \rightarrow DS_0$ is overestimated, as it is also for the $DS_1 \rightarrow DS_0$ transition energy for this excimer. Therefore, the observed tunability is more likely to originate from $DS_1 \rightarrow DS_0$ emission. The emission lifetime measurements for **4b** at 297 K in concentrated solution ($\lambda_{em} = 530$ nm) show a biexponential decay with a short 42 ns and long 153 ns component. In accordance with the theoretical calculations, the short component can be associated with the ^{1}MMLCT fluorescence and is the major component (82 %), with the longer-lived process associated with ^{3}MMLCT emission and phosphorescence. Moreover, in the thin film ($\lambda = 540$ nm) the short lifetime component increases to 89 ns (62 %), and the longer lifetime component shifts to 223 ns, suggesting phosphorescence from the ^{3}MMLCT state or possibly delayed fluorescence from ^{1}MMLCT.

The change in tunability of the emission energy is important from the perspective of future molecular design. The invariability of the PL maxima ($\Delta\lambda = 13$ nm) with donor–

© 2015 Wiley-VCH Verlag GmbH & Co. KGaA, Weinheim

acceptor strength over the series **4a–d** at low concentration, despite large changes in the electronic character of the ligands, is surely due to compensating effects in the electronic structure of the complexes that nullify the natural difference in electronic character of the substituents. Further detailed work is needed to clarify the origin of this outcome. However, a closer look at the leading orbitals of **3c**, **4c**, and **4c–4c** (Figure 5) shows significant changes in the electron densities from **4c** to **4c–4c**. The splitting between the bonding (d_{z^2}–d_{z^2}) and antibonding (d_{z^2}–d_{z^2})* levels shifts the (d_{z^2}–d_{z^2})* level to higher energy into the upper valence causing a systematic decrease in the $DS_1 \rightarrow DS_0$ emission energy and a red shift. At the same time the primary orbitals associated with the lowest-energy emission become more separated with the HOMO being entirely metal centered and the LUMO entirely ligand (pyridyl and/or substituent) centered. This leads to a larger substituent effect in the LUMO that is not compensated for in the HOMO as the bonding triazolate orbitals are no longer involved in the emission. On the other hand, density is observed on the triazole in both the LUMO and HOMO levels for **3c** and **4c** with clear and similar CT for both, considering the ligand space. Thus, although the enhanced tunability for the excimerization process can be demonstrated pictorially, the lack of tunability in the complexes themselves is more difficult to elucidate.

The current platinum(II) complexes demonstrate pronounced excimeric spectral shifts where the nature of the excited state has been fundamentally changed through specific metallophilic interactions. These interactions have been studied as a function of the nature of the substituent, revealing the effects of substitution on the excimeric equilibrium position and the emission energy as related to the donor–acceptor character of the ligand substituent. Further studies are warranted to understand more fully the excited-state dynamics and to achieve further control of luminescence as small singlet–triplet energy gaps are a key driver in the design of efficient emitters.

Keywords: charge transfer · density functional calculations · photoluminescence · platinum · stacking interactions

How to cite: *Angew. Chem. Int. Ed.* **2015**, *54*, 7949–7953
Angew. Chem. **2015**, *127*, 8060–8064

[1] a) W. Y. Wong, *Coord. Chem. Rev.* **2005**, *249*, 971–997; b) C. L. Ho, W. Y. Wong, *New J. Chem.* **2013**, *37*, 1665–1683.
[2] a) X. Yang, C. Yao, G. Zhou, *Platinum Met. Rev.* **2013**, *57*, 2–16; b) G. Cheng, S. C. F. Kui, W.-H. Ang, M.-Y. Ko, P.-K. Chow, C.-L. Kwong, C.-C. Kwok, C. Ma, X. Guan, K.-H. Low, S.-J. Su, C.-M. Che, *Chem. Sci.* **2014**, *5*, 4819–4830; c) C. F. Kui, P. K. Chow, G. S. M. Tong, S.-L. Lai, G. Cheng, C.-C. Kwok, K.-H. Low, M. Y. Ko, C.-M. Che, *Chem. Eur. J.* **2013**, *19*, 69–73.
[3] G. J. Zhou, Q. Wang, W. Y. Wong, D. Ma, L. Wang, Z. Lin, *J. Mater. Chem.* **2009**, *19*, 1872–1883.
[4] a) C. L. Li, Y. J. Su, Y. T. Tao, P. T. Chou, C. H. Chien, C. C. Cheng, R. S. Liu, *Adv. Funct. Mater.* **2005**, *15*, 387–395; b) M. Tavasli, S. Bettington, M. R. Bryce, H. A. A. Attar, F. B. Dias, S. King, A. P. Monkman, *J. Mater. Chem.* **2005**, *15*, 4963–4970; c) D. A. Sexton, L. H. Skibsted, D. Magde, P. C. Ford, *Inorg. Chem.* **1984**, *23*, 4533–4538; d) M. Sowinska, J. P. Launay, J. Mugnier, J. Pouget, B. Valeur, *J. Photochem.* **1987**, *37*, 69–79.
[5] a) A. Vlcek, Jr., H. B. Gray, *Inorg. Chem.* **1987**, *26*, 1997–2001; b) A. A. Vlcek, Jr., H. B. Gray, *J. Am. Chem. Soc.* **1987**, *109*, 286–287; c) A. E. Stiegman, S. F. Rice, H. B. Gray, V. M. Miskowski, *Inorg. Chem.* **1987**, *26*, 1112–1116; d) A. C. Durrell, G. E. Keller, Y.-C. Lam, J. Sykora, A. Vlcek, Jr., H. B. Gray, *J. Am. Chem. Soc.* **2012**, *134*, 14201–14207.
[6] a) H.-K. Yip, C. M. Che, Z.-Y. Zhou, T. C. W. Mak, *J. Chem. Soc. Chem. Commun.* **1992**, 1369–1371; b) S. W. Lai, M. C. W. Chan, T. C. Cheung, S. M. Peng, C. M. Che, *Inorg. Chem.* **1999**, *38*, 4046–4055; c) V. W. W. Yam, K. M. C. Wong, *Chem. Commun.* **2011**, *47*, 11579–11592; d) L. Murphy, P. Brulatti, V. Fattori, M. Cocchi, J. A. G. Williams, *Chem. Commun.* **2012**, *48*, 5817–5819.
[7] a) S. Y. Chang, J. Kavitha, S. W. Li, C. S. Hsu, Y. Chi, Y. S. Yeh, P. T. Chou, G. H. Lee, A. J. Carty, Y. T. Tao, C. H. Chien, *Inorg. Chem.* **2006**, *45*, 137–146; b) W. Lu, B. X. Mi, M. C. W. Chan, Z. Hui, C. M. Che, N. Zhu, S. T. Lee, *J. Am. Chem. Soc.* **2004**, *126*, 4958–4971.
[8] a) C. F. Chang, Y. M. Cheng, Y. Chi, Y. C. Chiu, C. C. Lin, G. H. Lee, P. T. Chou, C. C. Chen, C. H. Chang, C. C. Wu, *Angew. Chem. Int. Ed.* **2008**, *47*, 4542–4545; *Angew. Chem.* **2008**, *120*, 4618–4621; b) F. Q. Bai, T. Liu, X. Zhou, J.-P. Zhang, H.-X. Zhang, *J. Theor. Comput. Chem.* **2009**, *8*, 603–613.
[9] a) T. Y. Kim, A. B. S. Elliott, K. J. Shaffer, C. J. McAdam, K. C. Gordon, J. D. Crowley, *Polyhedron* **2013**, *52*, 1391–1398; b) P. D. Jarowski, Y. L. Wu, W. B. Schweizer, F. Diederich, *Org. Lett.* **2008**, *10*, 3347–3350.
[10] J. A. G. Williams, S. Develay, D. L. Rochester, L. Murphy, *Coord. Chem. Rev.* **2008**, *252*, 2596–2611.
[11] a) B. Tuesuwan, S. M. Kerwin, *Biochemistry* **2006**, *45*, 7265–7276; b) J. C. Loren, A. Krasiński, V. V. Fokin, K. B. Sharpless, *Synlett* **2005**, 2847–2850; c) X. Chen, X. Chen, Z. Zhao, P. Lü, Y. Wang, *Chin. J. Chem.* **2009**, *27*, 971–977.
[12] B. Zhang, B. Yan, *Anal. Bioanal. Chem.* **2010**, *396*, 973–982.
[13] a) K. J. Kilpin, E. L. Gavey, C. J. McAdam, C. B. Anderson, S. J. Lind, C. C. Keep, K. C. Gordon, J. D. Crowley, *Inorg. Chem.* **2011**, *50*, 6334–6346; b) J. Y. Lallemand, J. Soulié, J. C. Chottard, *Chem. Commun.* **1980**, 436–438.
[14] C. Hansch, A. Leo, R. W. Taft, *Chem. Rev.* **1991**, *91*, 165–195.
[15] a) W. H. Lam, E. S.-H. Lam, V. W.-W. Yam, *J. Am. Chem. Soc.* **2013**, *135*, 15135–15143; b) F. Mendizabal, *Int. J. Quantum Chem.* **2008**, *108*, 1164–1172; c) Gaussian 09 (Revision C01), see the Supporting Information, Section S7, for the complete reference.

Received: March 14, 2015
Published online: May 26, 2015

 © 2015 Wiley-VCH Verlag GmbH & Co. KGaA, Weinheim